A&A 595, A102 (2016)
DOI: 10.1051/0004-6361/201628764

Astronomy & Astrophysics

Detection of exposed H_2O ice on the nucleus of comet 67P/Churyumov-Gerasimenko

as observed by Rosetta OSIRIS and VIRTIS instruments

M. A. Barucci[1], G. Filacchione[2], S. Fornasier[1,3], A. Raponi[2], J. D. P. Deshapriya[1], F. Tosi[2], C. Feller[1,3], M. Ciarniello[2], H. Sierks[4], F. Capaccioni[2], A. Pommerol[5], M. Massironi[6], N. Oklay[4], F. Merlin[1,3], J.-B. Vincent[4], M. Fulchignoni[1,3], A. Guilbert-Lepoutre[7], D. Perna[1], M. T. Capria[2], P. H. Hasselmann[1], B. Rousseau[1], C. Barbieri[8], D. Bockelée-Morvan[1], P. L. Lamy[9], C. De Sanctis[2], R. Rodrigo[10,11], S. Erard[2], D. Koschny[12], C. Leyrat[1], H. Rickman[13,14], P. Drossart[1], H. U. Keller[15], M. F. A'Hearn[16], G. Arnold[17], J.-L. Bertaux[18], I. Bertini[19], P. Cerroni[2], G. Cremonese[19], V. Da Deppo[20], B. J. R. Davidsson[21], M. R. El-Maarry[5], S. Fonti[22], M. Fulle[23], O. Groussin[9], C. Güttler[4], S. F. Hviid[17], W. Ip[24], L. Jorda[9], D. Kappel[17], J. Knollenberg[17], J.-R. Kramm[4], E. Kührt[17], M. Küppers[25], L. Lara[26], M. Lazzarin[19], J. J. Lopez Moreno[26], F. Mancarella[22], F. Marzari[19], S. Mottola[17], G. Naletto[20], M. Pajola[27], E. Palomba[2], E. Quirico[28], B. Schmitt[28], N. Thomas[5], and C. Tubiana[4]

(Affiliations can be found after the references)

Received 21 April 2016 / Accepted 11 August 2016

ABSTRACT

Context. Since the orbital insertion of the Rosetta spacecraft, comet 67P/Churyumov-Gerasimenko (67P) has been mapped by OSIRIS camera and VIRTIS spectro-imager, producing a huge quantity of images and spectra of the comet's nucleus.
Aims. The aim of this work is to search for the presence of H_2O on the nucleus which, in general, appears very dark and rich in dehydrated organic material. After selecting images of the bright spots which could be good candidates to search for H_2O ice, taken at high resolution by OSIRIS, we check for spectral cubes of the selected coordinates to identify these spots observed by VIRTIS.
Methods. The selected OSIRIS images were processed with the OSIRIS standard pipeline and corrected for the illumination conditions for each pixel using the Lommel-Seeliger disk law. The spots with higher I/F were selected and then analysed spectrophotometrically and compared with the surrounding area. We selected 13 spots as good targets to be analysed by VIRTIS to search for the 2 μm absorption band of water ice in the VIRTIS spectral cubes.
Results. Out of the 13 selected bright spots, eight of them present positive H_2O ice detection on the VIRTIS data. A spectral analysis was performed and the approximate temperature of each spot was computed. The H_2O ice content was confirmed by modeling the spectra with mixing (areal and intimate) of H_2O ice and dark terrain, using Hapke's radiative transfer modeling. We also present a detailed analysis of the detected spots.

Key words. comets: individual: 67P/Churyumov-Gerasimenko – techniques: imaging spectroscopy – techniques: photometric – techniques: image processing – methods: data analysis

1. Introduction

Space exploration has triggered major progress in our understanding of comets beginning in March 1986 with the exploration of comet 1P/Halley by an armada of missions including the ESA Giotto mission (Reinhard & Battrick 1986). With the arrival of the ESA Rosetta mission at the comet 67P/Churyumov-Gerasimenko (67P) on July 2014, comets appear more complex and fascinating than ever. All the visited comets show a low visible albedo and heterogeneous surface (Barucci et al. 2011). However 67P and some other periodic comets reveal the presence of intriguing bright spots on the surface (Sunshine et al. 2006, 2012; and Li et al. 2013; Pommerol et al. 2015). To better understand the properties and composition of the comet 67P is one of the major objectives of the ESA Rosetta mission, and all on-board instruments have so far contributed with high quality and a precious quantity of data.

Since the orbital insertion of the Rosetta spacecraft, the comet nucleus has been mapped by both Optical, Spectroscopic, and Infrared Remote Imaging System (OSIRIS), and Visible InfraRed Thermal Imaging Spectrometer (VIRTIS) acquiring a huge quantity of surface images in different wavelength bands and spectra, and producing the most detailed maps at the highest spatial resolution of a cometary nucleus surface. The OSIRIS imaging system (Keller et al. 2007) is composed of the Narrow Angle Camera (NAC) designed to study the nucleus with 11 large band filters at different wavelengths from the ultraviolet (269 nm) to the near-infrared (989 nm), while the Wide Angle Camera (WAC) is devoted to the study of gaseous species in the coma with a set of 14 narrow band filters ranging from the ultraviolet to visible wavelengths. The OSIRIS imaging system was the first instrument capable of mapping a comet surface at high resolution, reaching a maximum resolution of 11 cm/px during the closest fly-by that occurred on February 14, 2015, at a distance of ~6 km from the nucleus surface. VIRTIS (Coradini et al. 2007) is composed of two channels: VIRTIS-M, a spectro-imager operating both in the visible (0.25−1.0 μm) and infrared (1.0−5.0 μm) ranges at low spectral resolution ($\lambda/\delta\lambda$ = 70–380), devoted to surface composition, and VIRTIS-H, a single-aperture infrared spectrometer (1.9−5.0 μm) with higher

spectral resolution capabilities ($\lambda/\delta\lambda$ = 1300–3000) devoted to the investigation of activity.

The OSIRIS images of 67P show a highly shaped, irregular bilobed comet, with a dark, dehydrated, and morphologically complex surface characterized by several terrain types, including numerous diverse geomorphologic features (Sierks et al. 2015). The comet's surface is highly heterogeneous with different geological terrains showing smooth, dust-covered areas, large scale depressions, brittle materials with many pits and circular structures, and exposed consolidated areas (Thomas et al. 2015a; El-Maarry et al. 2015, 2016). Pits have also been connected to activity, possibly accompanied by outbursts (Vincent et al. 2015). The complex surface of comet 67P shows regions covered by different layers of dust on both lobes, including areas with evidence of transport and redistribution of dust materials (Thomas et al. 2015b). Temporal variations of morphological structures have also been observed on the smooth terrains of the Imhotep region (Groussin et al. 2015), as well as in other regions (Fornasier et al. 2016), in particular when the comet was close to perihelion. The comet shows albedo variation of up to about 25% and spectrophotometric analysis (Fornasier et al. 2015) identified at least three groups of terrains with different spectral slopes (computed in the 535–882 nm range). These differences have been associated with the local composition variation, but since many different surface characteristics overlap, this makes the interpretation difficult. Oklay et al. (2016a) also studied surface variegation on the comet, detecting local color inhomogeneities connected to active and inactive surface regions.

The first results by VIRTIS (Capaccioni et al. 2015) about the spectral analysis showed the presence of a broad absorption feature around 2.9–3.6 μm present across the entire observed region and compatible with carbon-bearing compounds (opaque minerals associated with organic macromolecular materials) with no evidence of ice-rich patches. Later on, De Sanctis et al. (2015) detected the first evidence for the presence of H_2O ice as part of a diurnal cycle on the neck of the comet, while Filacchione et al. (2016a) identified H_2O ice on two gravitational debris falls in the Imhotep region exposed on the walls of elevated structures. The latter was interpreted as being possibly extended layering in which the outer dehydrated crust is superimposed over water ice-enriched layers. During the first mapping phase of 67P nucleus, completed in August–November 2014 (heliocentric distances between 3.6 and 2.7 AU), VIRTIS-M achieved a complete mapping of the illuminated regions in the equatorial and northern hemisphere, which enabled us to retrieve the first compositional maps by using VIS and IR spectral parameters (Filacchione et al. 2016b). During the same period, coma observations performed by VIRTIS-M (Migliorini et al. 2016) and VIRTIS-H (Bockelée-Morvan et al. 2015) channels have traced the H_2O vapor emission, which occurs preferentially above the illuminated regions of the northern hemisphere.

As limited evidence of exposed H_2O ice regions has so far been collected, the aim of this work is to investigate in depth the composition of the 67P surface, combining the high spatial resolution images of OSIRIS and the high spectral resolution of VIRTIS for detecting and emphasizing interesting ice spectral signatures. Over 100 m-sized spots were identified by Pommerol et al. (2015), possibly associated with the presence of H_2O, on the basis of laboratory experiments, but with no confirmation of the real presence of ice. Deshapriya et al. (in prep.) are collecting a catalogue of large bright spots that are present on the surface of the comet by analyzing the OSIRIS images and spectrophotometry data. For this work we selected the largest spots, good candidates to search for H_2O ice that could be detected at the lower angular resolution of VIRTIS. We identify large features with high albedo and low spectro-photometric slope with OSIRIS, we compute accurate coordinates, and we analyze them on the basis of the VIRTIS spectra. Over the large number of spots identified by OSIRIS, 13 of them were checked by VIRTIS. Eight of them show clear evidence of H_2O ice in their spectra.

In this paper we report on the analysis of the eight bright spots for which we obtained a positive detection of H_2O ice in VIRTIS data. In Sect. 2, the OSIRIS data and the performed analysis are presented and, in Sect. 3, the VIRTIS data, while in Sect. 4 the spectral modeling of the selected spots is described. In Sect. 5, a detailed analysis of the spots and surrounding area is reported, while in Sect. 6, a possible evolution of the area is discussed. The main aim of this work is to confirm the unambiguous presence of H_2O ice by spectral analysis.

2. OSIRIS data

Bright spots have been observed on 67P at various locations on the nucleus throughout the cruise phase of the Rosetta mission. First detections of these spots date back to as early as August 2014 and they continued to appear in numerous forms, be it an ensemble of a plethora of small bright spots, or much larger individual or twin bright patches. The abundance of these spots reached a peak during the perihelion passage of comet 67/P in August 2015, resulting in the largest white patches ever detected on the cometary nucleus. The first objective of this study is to explore the nature of these spots in terms of spectrophotometry.

We started by selecting potential bright spots found on OSIRIS NAC data with good spectro-photometry and spatial coverage. In the event of an observational sequence of several filters, owing to the fact that both the spacecraft and cometary nucleus are constantly in motion, the recorded images do not necessarily show exactly the same field of view. Owing to the time difference between a pair of consecutive images being around ten seconds, there is a small shift in the fields of view. Hence we have to take this shift into account when stacking up images and creating a data cube for spectral analysis. To achieve this, we adopted an algorithm that automatically identifies identical features in consecutive images and estimates the affine transformation matrix between each couple of consecutive images (ORB and RANSAC tools implemented by van der Walt et al. 2014). Then we analyzed the data cubes to identify bright spots. The basic criterion to identify these spots was their high reflectance compared to the typical nucleus in the filter wavelengths observed. We note that the data used are from 3B level of the standard OSIRIS data reduction pipeline, which accounts for the correction for bias, flat field, geometric distortion, solar flux, and calibration in absolute flux (Tubiana et al. 2015). Thus the data available in the reduced files are in the form of radiance factor that corresponds to the ratio between the observed scattered radiance (I) from the comet and incoming solar irradiance (F_λ) at the heliocentric distance of the comet, being referred to as the I/F value

$$I/F(\lambda) = \frac{\pi I(i, e, \alpha, \lambda)}{F_\lambda}, \quad (1)$$

where i is the incident angle, e is the emission angle, and α is the phase angle.

Next we proceeded to generate synthetic images to correct for the illumination conditions and observational geometry using the OASIS tool (Jorda et al. 2010) and the shape model SHP5

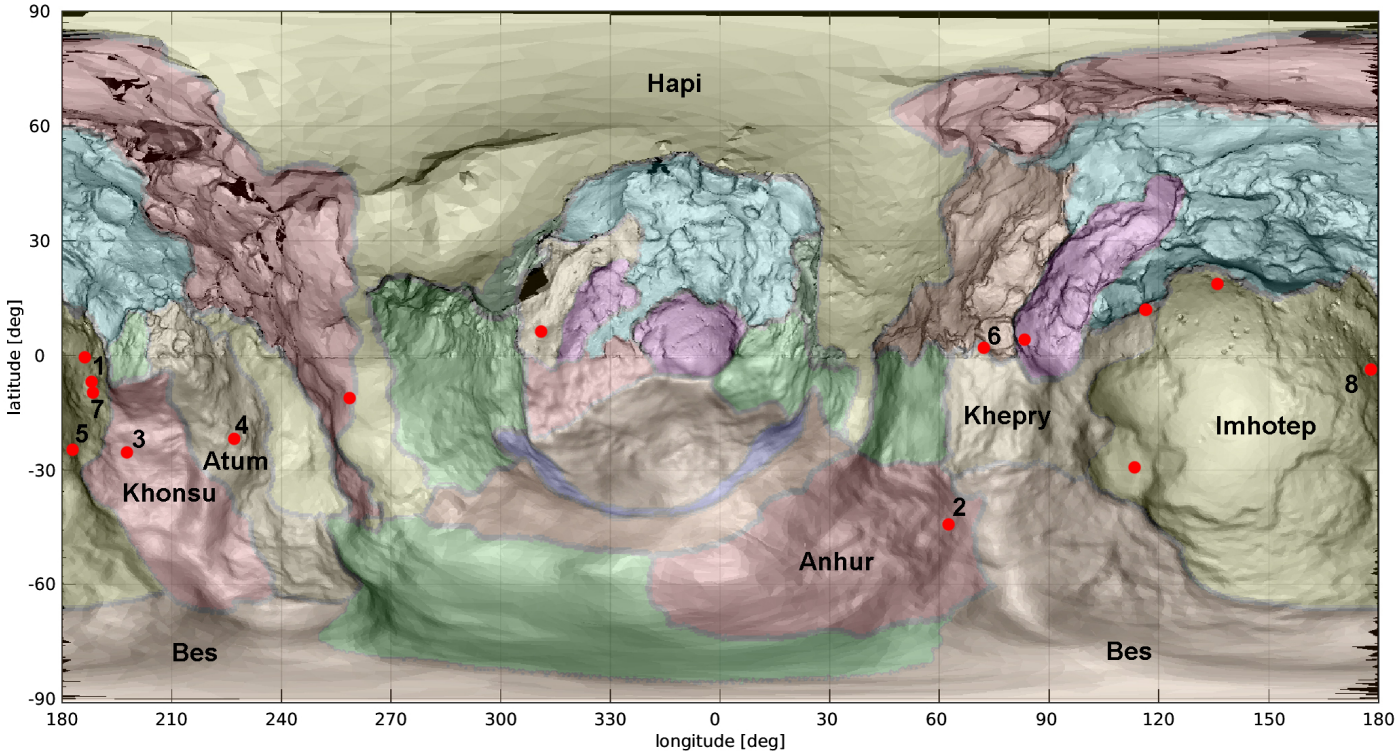

Fig. 1. Map of comet 67P/Churyumov-Gerasimenko, resulting from merging a more detailed shape model SHAP4S (Preusker et al. 2015) for the northern hemisphere and shape model SHAP5 (Jorda et al. 2016) for the southern hemisphere. In red the selected bright spots are reported, based on OSIRIS images and a spectro-photometric analysis, considered as good targets to be investigated by an analysis of VIRTIS data, plus the two bright spots analysed by Filacchione et al. (2016a). The numbers (1–8) represent the spots with positive detection of H_2O ice by VIRTIS analysis discussed in this paper.

(Jorda et al. 2016). This yields incident and emission angles for each pixel, which enables us to apply the Lommel-Seeliger disk law

$$D(i,e) = \frac{2\cos(i)}{\cos(i)+\cos(e)} \quad (2)$$

$$(I/F)_{\rm corr}(\alpha,\lambda) = \frac{\pi I(i,e,\alpha,\lambda)/(F_\lambda)}{D(i,e)}. \quad (3)$$

Derived from I/F plots we also produced relative reflectance plots with radiance factors normalized to a given filter (i.e. *F23*, green filter at 535 nm), enabling us to get an insight into the composition of the areas sampled for this analysis. As the ice displays a flatter spectrum in comparison to the red nature of organic-rich typical comet's nucleus material, we set the following criteria for the bright spots to qualify as final candidates: i) higher albedo properties than the typical nucleus I/F and ii) flat spectral behavior, compared to the typical nucleus on relative reflectance plots.

The above method enabled us to filter potential candidates and discard certain previously catalogued bright spots that had shown higher albedo properties, but not necessarily having flat spectral behavior when normalized, thus failing to meet the second requirement. In this case, the high albedo properties were probably due to the illumination conditions during the observation.

We selected 13 spots (or cluster of spots) reported in the map (Fig. 1) as the best sample to be analysed by spectroscopy with VIRTIS. In this paper we present only eight spots (Table 1) for which VIRTIS spectral analysis gave positive detection of H_2O ice signatures. The OSIRIS images of the area and the zoom of the selected eight bright spots were reported in Fig. 2, together with the measured I/F and the relative spectro-photometry reflectance. As shown in Fig. 2, the spots 4 (depending on the shadow), 6, and 7 belong to a cluster.

3. VIRTIS data

The search of VIRTIS-M spectra in correspondence with the bright albedo features identified on OSIRIS images needed a deep data mining of the dataset. Since the entire nucleus was imaged with very high redundancy from a wide range of distances, local times and illumination/viewing geometries, the research has been performed starting from georeferenced data. For each individual pixel in each VIRTIS-M observation, many geometry parameters, including longitude, latitude, incidence, emission, phase angles, distance, and local solar time for the pixel center and four corners, were computed by means of SPICE (Acton 1996) routines that are able to reconstruct these quantities starting from spacecraft and comet attitude and trajectory kernels. Once computed and validated by the VIRTIS team, these geometry (.GEO) cubes are released through ESA's PSA archive and made publicly available. The nucleus shape model used for computation is SHAP5, derived from OSIRIS images by using a stereophotoclinometry method (Jorda et al. 2016). The coordinates grid is based on the Cheops frame (Preusker et al. 2015). Some examples of geometry parameters computed for VIRTIS-M nucleus observations are given in Filacchione et al. (2016b). The geometry information relative to each pixel is therefore ingested in a database.

Table 1. Observing conditions for the OSIRIS images as reported in Fig. 2, where the ice spots have been identified.

N.	Time reference	Filters	d (m)	Region	α (°)	Δ (km)	R (m/px)	Lat (°)	Long (°)
1	2015-06-27T13h26	$F22, F23, F41, F24, F71, F27, F51, F61, F28, F15$	36	Imhotep	89.50	191.94	3.6	−5.8	189.4
2	2015-06-27T17h48	$F22, F23, F41, F24, F71, F27, F51, F61, F28, F15$	45	Anhur	89.39	188.43	3.5	−41.7	63.7
3	2015-04-12T21h42	$F22, F23, F41, F24, F71, F27, F51 F61, F28, F16, F15$	11	Khonsu	80.46	147.98	2.7	−23.8	198.3
4	2014-11-22T04h57	$F22, F23, F24, F27, F28, F51, F61$	10	Atum	92.70	29.50	0.54	−20.7	227.4
5	2014-11-22T06h32	$F22, F23, F24, F27, F28, F51, F61$	6.5	Imhotep	92.78	29.50	0.54	−22.0	182.8
6	2014-09-19T09h19	$F22, F16, F23, F24, F41$	2–5 (each)	Khepry	70.48	26.50	0.49	4.2	71.7
7	2014-09-05T05h21	$F22, F23, F27, F16, F28, F41, F71$	3–5 (each)	Imhotep	57.23	41.44	0.77	−8.1	188.3
8	2014-09-05T08h00	$F22, F23, F27, F16, F28, F41, F71$	6	Imhotep	58.43	40.76	0.75	−2.4	174.8

Notes. The time (UT) refers to the start time of the first image of each sequence, followed by the number of filters available. The diameter size (d) of the spots along with the location region, phase angle (α), distance between Rosetta spacecraft and comet surface (Δ), spatial resolution (R), latitude (Lat), and longitude (Long) are reported.

3.1. Search for the 2 μm absorption feature

Using the method described above, the search of VIRTIS-M pixels located in correspondence with the bright spot coordinates identified on OSIRIS images was performed. As a general rule, we selected all VIRTIS-M pixels within a radius of 2° in longitude and latitude around the position estimated on the OSIRIS images. The corresponding reflectance spectra are grouped together to form a spectrogram (Filacchione et al. 2016a), one for each MTP, and then further processed by calculating the 2 μm band depth, used as a proxy to determine the presence of H_2O ice on the surface in the case of values that were larger than a 5% threshold. Water ice reflectance shows diagnostic absorptions at 1.5, 2.0 and 3.0 μm. The decision to use only the 2 μm band as a proxy to identify the presence of water ice on 67P surface was driven by two different requirements: (i) the 1.5 μm band is partially corrupted by the presence of an instrumental order-sorting filter, which makes it difficult to retrieve a correct band shape, particularly for pixels close to sharp illumination transitions and shadows; (ii) the intense 3 μm band has a complex shape owing to the overlapping of the water and organic material absorptions, which causes changes in shape, center, and depth, depending on the relative abundances of the two end-members. Conversely, the 2 μm spectral range is not influenced by similar effects. Moreover, the 2 μm band is well-defined for a wide range of grain sizes, making it a good spectral marker to identify the presence of water ice.

As a general rule, the detection of the H_2O ice on a given place can be limited by unfavorable instrumental signal-to-noise conditions, spatial resolution on ground and oblique illumination/viewing geometry. A summary of the observations showing a positive identification of the 2 μm H_2O ice-band feature is given in Table 2. Infrared color images of the eight spots are shown in Fig. 4, together with the observed reflectance spectra and best spectral fits, as discussed later in Sect. 4. In absence of water ice, VIRTIS spectra correspond with the Dark Terrain unit, as reported in Fig. 3, which shows a featureless red slope in the 1–2.6 μm range and an intense organic material absorption band at 3.0 μm.

3.2. Temperature of the icy spots

For each spot we identified VIRTIS-M observations showing the eight spot areas imaged with the best illumination and viewing geometries to maximize the S/N ratio. The VIRTIS-M dataset considered in this work is summarized in Table 3.

Surface temperature is derived from VIRTIS-M infrared data by modeling the 4.5–5.1 μm spectral radiance (at the pixel where the spectrum has the deepest content of H_2O ice) with a Bayesian approach (Tosi et al. 2014). On the surface of the nucleus, the temperature of each point is generally a function of local thermophysical properties (albedo, composition, grain size, roughness, thermal conductivity, volatiles sublimation) and instantaneous illumination conditions (solar incidence angle, or true local solar time). All measurements considered in this work were acquired by VIRTIS-M in the local solar timeframe between late morning to early afternoon, with pixel resolution ranging between 5.0 and 23.5 m/pixel. In these conditions, H_2O ice-rich spots show temperatures ranging between about 158 and 218 K. Since the comet's surface is not isothermal, because of local roughness, the temperature values retrieved by VIRTIS should be considered representative only of the warmest fraction of the pixel, corresponding to the more illuminated areas. Moreover, the instrumental noise-equivalent temperature is about 150 K, corresponding to the minimum temperature detectable by the instrument. The error associated with the temperatures reported in Table 3 are between ±30 K for the measurement at minimum temperature T = 158 K, and ±10 K for the one at maximum T = 218 K.

4. Spectral modeling

To derive the properties of the H_2O ice detected in the bright spots on the surface of the comet, a spectral analysis was performed using Hapke's radiative transfer model (Hapke 2012), as described in Ciarniello et al. (2011). Unfortunately we are still not able to infer the real composition of the organic-rich dark terrain present on the comet surface. The broad absorption band centered at 3.2 μm, and the difficulty of its interpretation, have been largely discussed by Quirico et al. (2016) on the basis of present knowledge of the composition of cometary grains and all the components available in laboratory data. The mixture presented in this paper was consequently modeled by means of two spectral end members: crystalline water ice, simulated by using optical constants measured at T = 160 K between 1 and 4 μm (Warren et al. 1984; Mastrapa et al. 2008, 2009; Clark et al. 2012) and a Dark Terrain unit corresponding to the average spectrum of the comet's surface after the application of photometric correction (Ciarniello et al. 2015), as shown

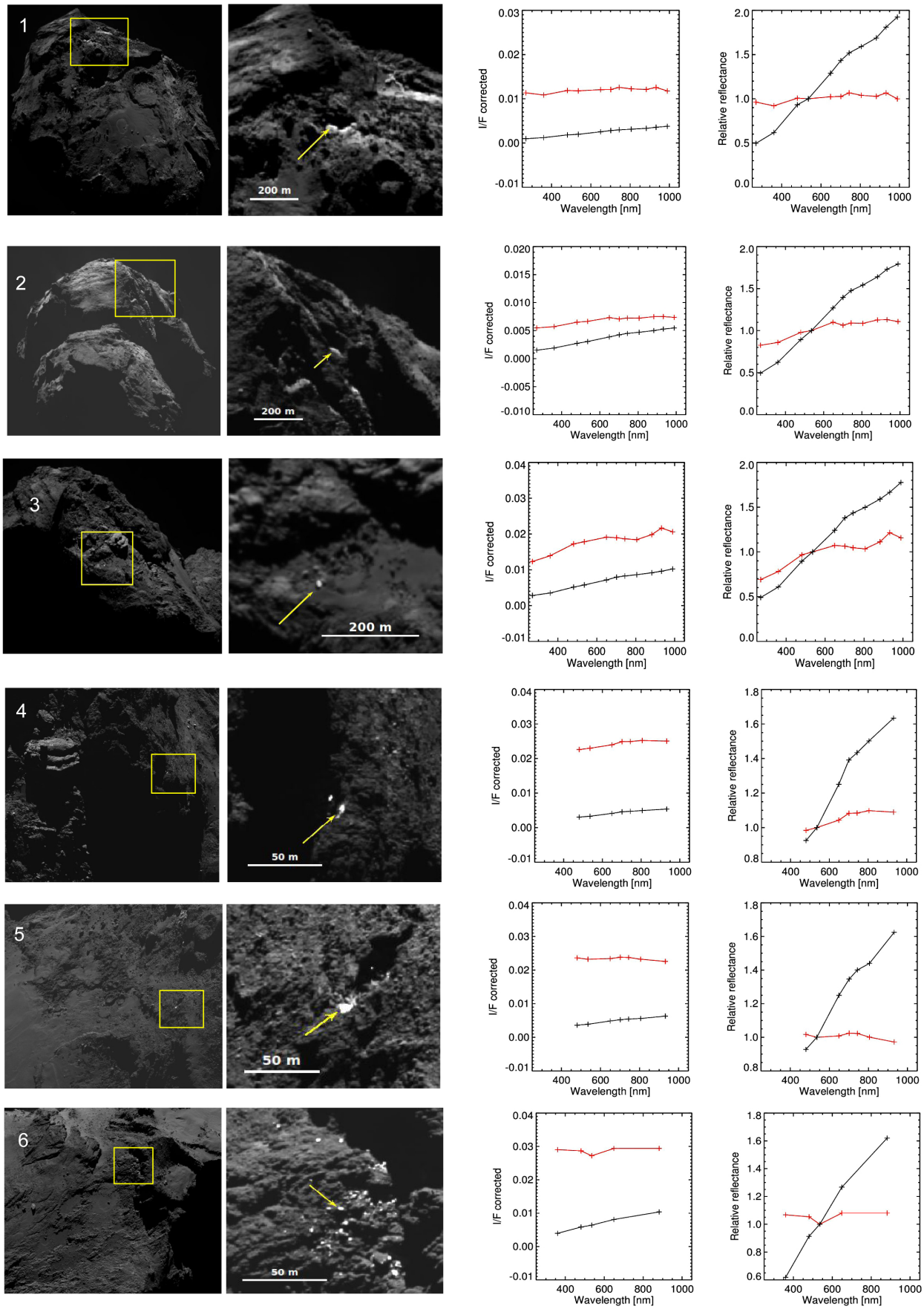

Fig. 2. NAC OSIRIS images (*first column*) for the eight spots reported in Table 1 with a zoom on the spot (*second column*). The images have been taken with $F22$ filter (at 649.2 nm). The arrows indicate the spots that have been analysed using boxes of 3×3 pixels. The measured $I/F(\alpha)$ of the bright spots are reported in red, while the surrounding area is reported in black (*third column*). The relative reflectance (normalized to $F23$ at 535 nm) of the indicated bright spot in red and the surrounding area in black are represented in the *fourth column*.

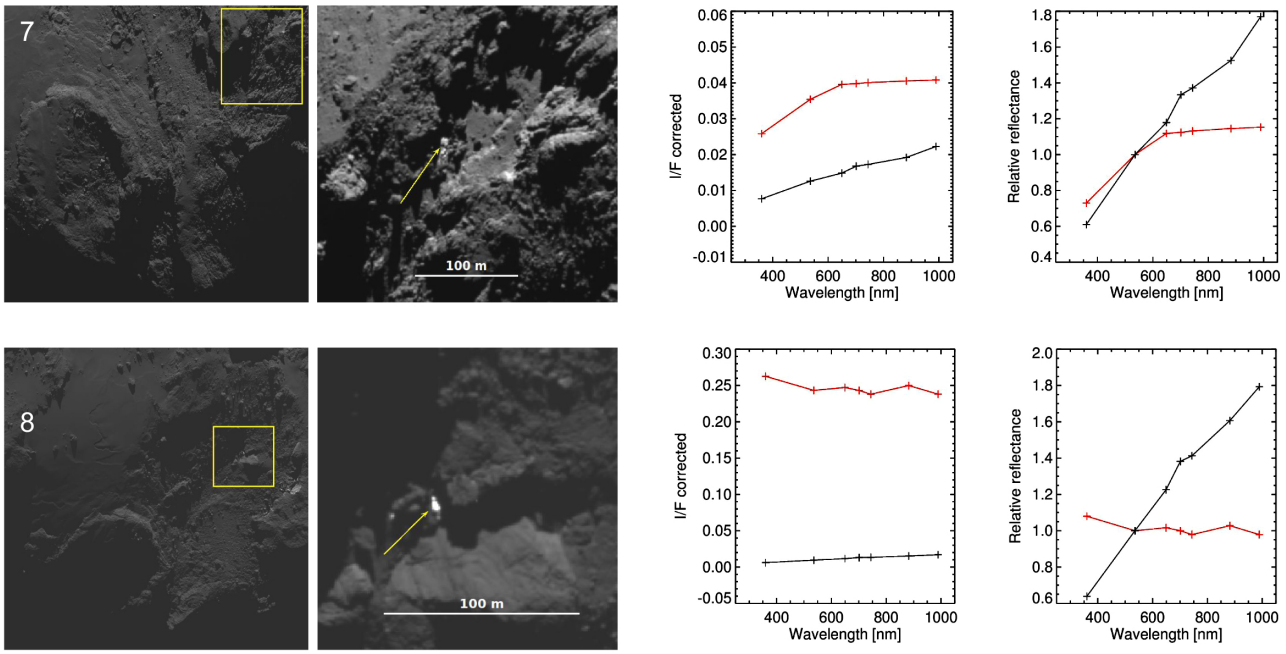

Fig. 2. continued.

Table 2. Coverage of OSIRIS bright spot locations in VIRTIS dataset and [number] of 2 μm absorption band positive identifications.

OSIRIS Spot	Ice spot N.	MTP007	MTP008	MTP009	MTP010	MTP011	MTP012	MTP013	MTP014	MTP015	Total
nl1-5b	1	20 [0]	0	0	0	0	0	15 [2]	139 [0]	89 [0]	**2**
nl2-7b	-	0	0	0	40 [0]	0	16 [0]	15 [0]	8 [0]	8 [0]	**0**
nl3-12b	-	149 [0]	0	36 [0]	144 [0]	64 [0]	0	32 [0]	77 [0]	87 [0]	**0**
nl4-13	2	0	0	0	0	0	0	4 [0]	106 [9]	49 [0]	**9**
nl5-16	-	142 [0]	0	0	32 [0]	26 [0]	0	45 [0]	121 [0]	70 [0]	**0**
nl6-17a	3	0	0	0	0	0	0	15 [0]	116 [9]	64 [3]	**12**
nl7-19	4	0	0	195 [32]	0	0	0	29 [0]	52 [0]	39 [0]	**32**
nl8-20	5	40 [0]	0	0	300 [86]	0	0	38 [0]	190 [0]	87 [0]	**86**
nl9-22	-	225 [0]	0	140 [0]	86 [0]	0	0	21 [0]	77 [0]	59 [0]	**0**
nl10-23b	-	0	0	0	0	0	27 [0]	184 [0]	58 [0]	27 [0]	**0**
nl11-14b	6	102 [3]	711 [0]	72 [0]	140 [0]	70 [0]	0	46 [0]	76 [0]	65 [0]	**3**
nl12-24	7	94 [10]	0	0	0	0	0	14 [0]	122 [4]	66 [1]	**15**
nl13-25	8	326 [0]	0	0	345 [3]	41 [0]	0	43 [0]	93 [0]	85 [0]	**3**

Notes. MTPs are Rosetta mission medium term plan time intervals, each one having a duration of about one month (MTP7 corresponds to September 2014, MTP15 to April 2015). In the last column, the total positive detections are reported.

Table 3. Summary of VIRTIS-M dataset processed in this work.

N.	Observation name	Cube Parameters	Start time (UT)	End time	Phase (deg)	Incidence (deg)	Emission (deg)	Δ (km)	LST (h)	T (K)
1	I1_00383518966	432, 256, 158	2015-02-25T21:04:00	2015-02-25T21:30:19	53.02	66.94	41.92	81.51	12.23	203
2	I1_00385906923	432, 256, 70	2015-03-25T12:23:18	2015-03-25T12:46:34	73.49	67.08	45.83	88.23	15.20	197
3	I1_00385885107	432, 256, 70	2015-03-25T06:19:42	2015-03-25T06:42:58	74.47	53.03	31.27	94.06	12.43	218
4	I1_00373462192	432, 256, 86	2014-11-01T11:31:03	2014-11-01T11:45:22	103.07	60.11	43.28	32.39	11.04	168
5	I1_00377182711	432, 256, 80	2014-12-14T12:59:43	2014-12-14T13:13:02	91.77	43.41	52.15	19.44	15.44	188
6	I1_00376302211	432, 256, 80	2014-12-04T08:24:43	2014-12-04T08:38:01	91.07	57.34	70.64	23.49	14.81	179
7	I1_00369356914	432, 256, 109	2014-09-14T23:09:43	2014-09-14T23:45:57	66.89	78.22	30.26	28.16	11.03	163
8	I1_00377184571	432, 256, 74	2014-12-14T13:30:43	2014-12-14T13:43:02	92.66	48.30	54.87	19.92	15.59	158

Notes. For each spot, we report the observations offering the best signal-to-noise conditions with the pixel position (sample and line) reported in Table 4. For each pixel, basic information about observation time, geometry conditions, distance between the Rosetta spacecraft and comet surface (Δ), Local Solar Time (LST), and retrieved temperature (T) are given. The integration time is 3 s for all data reported. The cube parameters indicate the size of the acquisition in bands, sample, line dimensions.

in Fig. 3. The quantitative analysis is based on the spectral shape of the diagnostic absorption bands of H_2O ice. The absolute level of reflectance of the model is multiplied by a free parameter to fit the data, to account for uncertainties on the radiometric and photometric accuracy as well as errors on the local geometry information, owing to unresolved shadows and roughness. In some cases, the measured spectra present a fictitious slope where a high signal contrast is measured between adjacent pixels, like

Table 4. Parameters retrieved by modeling for each bright area.

Spot	VIRTIS file sample, line	Mixing modalities Alternative/Simultaneous		H_2O ice abundance (%)	H_2O ice grain size (μm)	Additional slope (%μm^{-1})	Goodness χ^2
1	I1_00383518966 s: 184, l: 24	areal intimate	A	1.1 1.2	350 450	5.2	4.19 4.16
2	I1_00385906923 s: 173, l: 42	areal intimate	A	0.1 0.5	40 200	no	1.18 1.04
3	I1_00385885107 s: 120, l: 35	areal intimate	A	1.3 1.8	750 1300	−2.8	2.78 3.30
4	I1_00373462192 s: 93, l: 35	areal intimate	S	3.2 4.0	4500 30	no	0.45
5	I1_00377182711 s: 61, l: 69	areal intimate	A	1.7 2.0	400 800	−4.0	1.47 2.15
6	I1_00376302211 s: 16, l: 38	areal intimate	S	1.9 1.0	6500 250	−1.8	0.28
7	I1_00369356914 s: 239, l: 66	areal intimate	A	1.5 1.8	10 15	−4.0	0.90 0.86
8	I1_00377184571 s: 6, l: 7	areal intimate	A	0.3 0.7	900 2200	no	0.56 0.55

Notes. The relative error on abundance and grain size is 40%, as estimated in Raponi (2014).

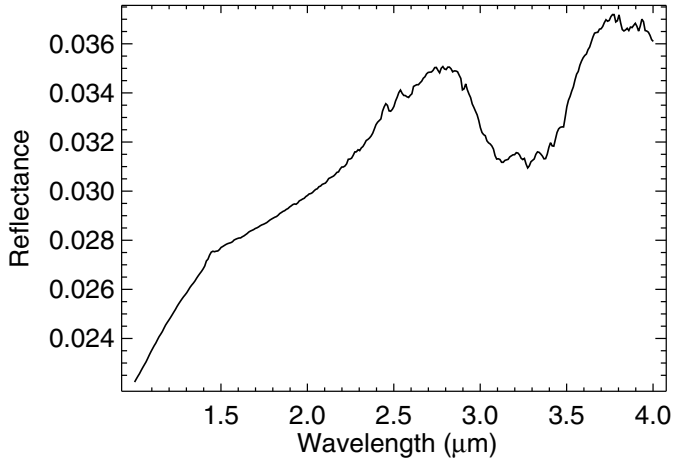

Fig. 3. Spectrum of Dark Terrain unit that corresponds to the average spectrum of the comet's surface.

regions near shadows. This is due to the increasing FWHM of the point spread function toward longer wavelength. To account for this effect, a slope is added to the model to fit the measured spectrum, where it is required. Because of its artificial origin it should not be the subject of interpretation. Before fitting, the observed spectra are corrected for spikes and instrumental artifacts. Thermal emission is modeled and removed simultaneously to the spectral fit, as in Protopapa et al. (2014). The best-fitting result is obtained by applying the Levenberg-Marquardt method for non-linear least squares multiple regression. During the fitting procedure, the spectral bands are weighted for the Poissonian noise as calculated in Raponi (2014). We have modeled areal and intimate mixing modalities: in the areal mixing, the surface is modeled as patches of pure H_2O ice and dark terrain; in the intimate mixing model the particles of the two end-member materials are in contact with each other. The model's free-parameters are the percentage and grain size of the water ice. Further details about spectral modeling are given in Filacchione et al. (2016a) and in Raponi et al. (2016). Most of the icy regions can be described by both areal and intimate mixture, which can be alternative. In the intimate mixing case, the model always requires larger abundance and grain size than the areal mixing case to compensate for the lack of the multiple scattering contribution, which is low because of the interaction of light with the dark terrain. The two alternative solutions indicated with A in Table 4 are the extremes of a possible set of solutions in which both kind of mixtures can be present simultaneously. For the spectra indicated with S in Table 4 (spots 4 and 6), we have only one possible solution in which the two kinds of mixtures both contribute to the production of the model, and two populations of grain size are modeled at the same time, confirming the result of Filacchione et al. (2016a). Figure 4 shows spectra and images for each spot with positive identification of ice using VIRTIS-M data. The best fitting model (in red) for each spot is shown as the areal mixing case, or the areal-intimate case according to the parameters, as indicated in Table 4.

To highlight the effect of variation in abundance and grain size of the water ice, in Fig. 5 we show, as an example, the best fit obtained for spot 3, in the areal mixture case, varying the H_2O ice abundance and the grain size. An additional slope has been set as a free parameter to obtain the best fit. The parameters used and the resulting goodness-of-fit of the models are shown in Table 5.

5. Analysis of the exposed H_2O ice spots

We analyze the OSIRIS NAC images in the areas where the spots have been identified and, in addition, we investigate all available observations to evaluate the lifetime of the H_2O ice spots. All spots are almost in equatorial or near-equatorial locations.

Spot 1. This bright feature is located in the southern hemisphere close to the Khonsu-Imhotep boundary and the cometary equator. The bright spot appears as a freshly exposed cliff on a rough region of rocky appearance bounding an alcove. It is likely a remnant of a collapsed sector of a former pit. The first detection of this feature occurred on 5 June 2015, when it measured 57 m, whereas later on, on 27 June 2015, it measured about 36 m.

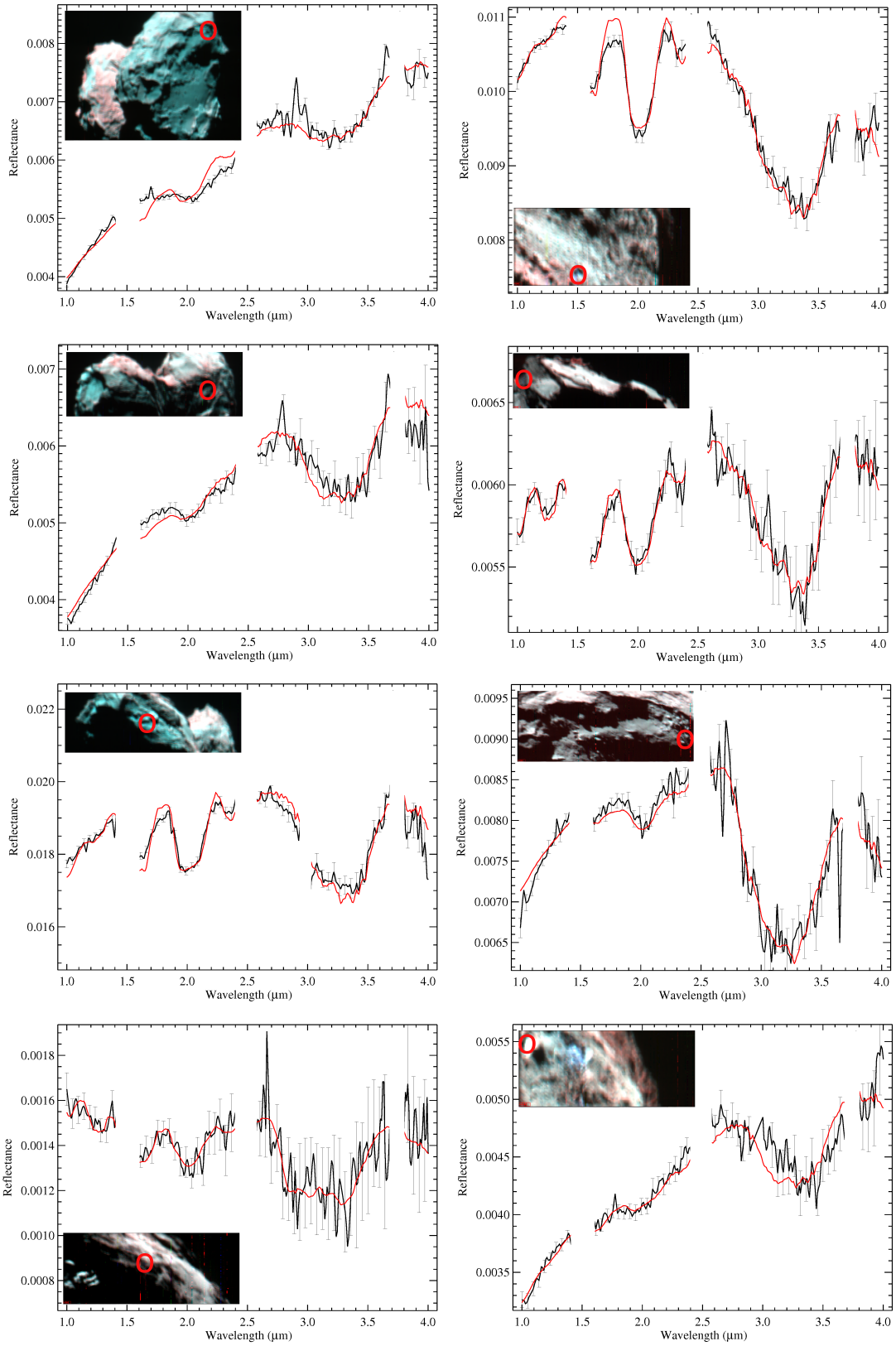

Fig. 4. VIRTIS-M infrared data of the eight spots. Spots 1–4 are shown in the *left column* from *top to bottom*. Spots 5–8 in the *right column* from *top to bottom*. Infrared images in the insert of the plot are built from a combination of spectral bands taken at 1.32 μm (B channel), 2.0 μm (G), 4.0 μm (R). For each spot, we report the VIRTIS-M observed reflectance (black curve), not corrected for phase angle, and best fit (red curve) as derived from the pixels reported in Table 3 and indicated by red circles on the images. The gaps in the spectral ranges correspond to order-sorting filter-junction wavelengths that can produce unreliable features and, for this reason, are not taken into account in the analysis.

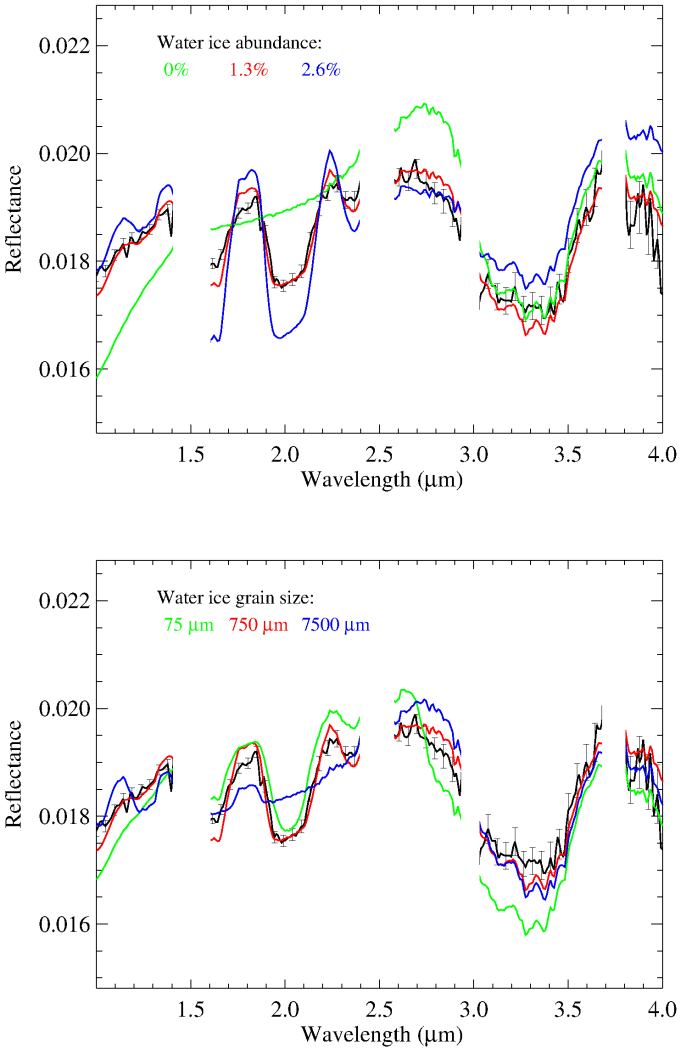

Fig. 5. Simulated reflectance spectra are shown to highlight the effect of variation in abundance and grain size of the water ice. In *both plots*, the black curve is the spectrum of spot 3, and the red curve is the best fit for areal mixture case already reported in Fig. 4. The green and blue curves are simulated by varying one of these parameters, as indicated: the *panel on the top* shows the effect of the variation in abundance of H_2O ice (0%, 1.3%, 2.6%) fixing the grain size at 750 μm, and the *panel on the bottom* shows the variation in grain size (75 μm, 750 μm, 7500 μm), fixing the H_2O ice abundance at 1.3%. The gaps in the spectral ranges are not taken into account, as in Fig. 3.

Spot 2. Located in the Anhur region in the southern hemisphere of the comet, this bright feature measures about 45 m. Owing to the oblique observing geometry and many shadows cast in the neighboring terrain, it is difficult to give a clear depiction of the surroundings. Nevertheless the feature seems to correspond to a flat terrace at the centre of a roundish area (possibly a collapsed pit) in a region of consolidated materials. It shows a very low albedo for a bright feature, although it stands out from that of the typical nucleus. The OSIRIS NAC observations of this bright spot are recorded from 4 June 2015 up to 11 July 2015. Similar to the case of spot 1, this feature is also surrounded by many shadows caused by the rugged terrain of Anhur.

Spot 3. This spot appears as a bright boulder close to a pancake-like feature (apparently composed of three broad layers), which is a morphologically unique feature right in the center of the Khonsu region (El-Maarry et al. 2016). The bright spot has a good temporal coverage in terms of OSIRIS NAC observations. It has been observed on several occasions from the end of March to the beginning of May in 2015. The observations suggest a diminution of its size from about 18 m in late March by about 8 m in April, up to complete disappearance in May. By applying illumination correction using the Lommer-Seeliger disk law, the reflectance of the bright spot increased by a factor of 2 for the sequence on 25 March, unlike other cases of bright features, with the exception of spot 8.

Table 5. Parameters used to perform the models shown in Fig. 5.

H_2O ice abundance (%)	H_2O ice grain size (μm)	Additional slope (%μm^{-1})	Goodness χ^2
1.3	750	−2.8	2.78
0	750	−4	31.2
2.6	750	0	15.0
1.3	75	−2.5	9.4
1.3	7500	−3.9	6.8

Notes. The first line represents the best fit (reported in Table 4) shown in red in both panels of Fig. 5. The abundance and grain size of water ice in areal mixture are fixed as: 0% and twice the abundance retrieved for the best fit, and one tenth and ten times the grain size retrieved for the best fit. The additional slope (free parameter of the model) and the resulting goodness are indicated in the table.

Spot 4. The OSIRIS NAC observations of 22 November 2014 reveal a cluster of bright features located at the Atum region margin close to its boundaries with the Khonsu and Anubis regions. The bright features seem to be freshly exposed brittle materials (El-Maarry et al. 2015) in a rocky-like area. The bright patches of varying individual sizes span an area of about 25 m in diameter. The largest patch appears to be about 10 m in size in this observation. Further analysis, including earlier images, reveals that this feature was observed as early as 2 September 2014. In the meantime the latest appearance of this feature on OSIRIS NAC observations was on 23 November 2014.

Spot 5. This bright spot faces the rounded feature with a diameter of 500 m in Imhotep, which is interpreted by Auger et al. (2015) as a fractured accumulation basin. Similar to the bright patches of spot 4, this patch also seems to be formed by a freshly exposed area of a highly fractured material. This bright spot was observed on 22 November 2014 and measures about 10 m. It has also been noted (Pommerol et al. 2015) that this bright feature was spotted as early as 5 September 2014 by OSIRIS NAC. It has also been included in the Oklay et al. (2016a) study. On further analysis of the images, it is possible to find the same feature in some images on 23 August 2014, but with a smaller size.

Spot 6. This is a cluster of small bright spots located in the Khepry region at the base of a scarp bordering a roundish flat terrace covered by dust deposits at the Babi region margin. Again the material, where the bright patches are located, appears consolidated, brittle (El-Maarry et al. 2015), and dissected by pervasive fractures. The bright patches themselves seem to be either on freshly exposed outcropping material or on boulders. These spots have been observed many times from late August 2014 through to the end of November 2014 by OSIRIS NAC. The first observation on 26 August 2014 indicates the presence of around some 20 small bright spots with sizes ranging from 1.5 m to 3 m along with few spots of about 6 m in size. The following observations on 5 September reveal that there has not been any significant change in the bright patches in terms of their sizes and population. There were more observations on 16 September and three days later (Pommerol et al. 2015), suggesting the stability of the

bright patches over time. Later on, an observation sequence on 29 October 2014 suggests that the cluster has reduced to only four bright spots, each measuring about 1 m, but it is not possible to rule out the possibility that some small bright spots may be under a shadow and hence not observable. Another sequence, on 22 November, reveals the cluster of bright spots present on observations in early September, leading to the conclusion that the observation on 29 October was subject to shadows. This cluster of bright spots seems to have been stable for at least three months.

Apart from this cluster of bright patches in late 2014, few observations dated from 25 March 2015 indicate the re-emergency of small bright patches at the same location. Despite the shadowy terrain, it is possible to discern up to three small bright patches, each about 5 m in diameter. Perhaps it could be inferred that this locality near the cliff at the Khepry/Babi border is active in terms of bright patches. Some mechanism may have triggered an outburst of icy material underneath the surface of this region allowing the cluster of bright patches to become apparent, possibly gravitational falls of boulders (Pajola et al. 2015) with consequent exposure of patches at the scarp foot.

Spot 7. This is a cluster of small bright patches that might correspond to a series of boulders at the base of a small terrace bounded by scarps. This feature appears on the OSIRIS NAC observations of 30 September 2014. It is located on a slope adjacent to the smooth plain in Imhotep, pointing to the neighboring Apis region. The location itself is somewhat shadowy and is camouflaged by the surrounding terrain, making it challenging to observe the full extension of this feature. VIRTIS-M data support the presence of H_2O ice for this bright feature located in Imhotep region with a size of about 5 m. The corresponding positive VIRTIS-M observations date back to early September 2014, suggesting that this bright feature has been on the cometary surface even as early as the beginning of September. Therefore this feature could have a lifespan of at least one month.

Spot 8. This Imhotep-based bright feature is recorded in several epochs. The bright spot is close to the isolated accumulation basin and to the small roundish features interpreted by Auger et al. (2015) as ancient degassing conduits. It is located at the base of what appears to be an open trench surrounded by steep small scarps. Therefore the full view of this feature is somewhat hampered by the constant casting of shadows and the viewing geometry. Nevertheless the multiple observations offer partial views of the feature that seems to lie on a consolidated flat area with fractures and tiny staircase borders. For example on the image recorded on 30 September 2014, it appears to be composed of two segments with one measuring 3 m, while the other measures 6 m approximately. We note that the absolute reflectance of this bright spot increased by a factor of 3 upon applying the illumination correction using Lommer-Seeliger disk law for the observation sequence on 5 September 2014. A similar effect has only been noticed in the case of spot 3, where the factor was 2. The earliest detection of this feature dates to 25 August 2014 and the corresponding positive VIRTIS-M recordings date to mid-December 2014, suggesting a stable existence of almost four months on surface for this bright feature.

6. Temporal evolution of the bright spots

Although only a subset of the bright spots detected by OSIRIS can be analyzed by VIRTIS, the unambiguous detection of the spectral signatures of H_2O ice in eight of these bright spots is a clear confirmation of their icy nature. In Sect. 5, we detail evidence of spots with long life time. Here (Fig. 6) we add a comparison for a cluster of bright spots (spot 6) in Khepry with observations at an interval longer than two months, which confirms the stability of this cluster at that time of the mission.

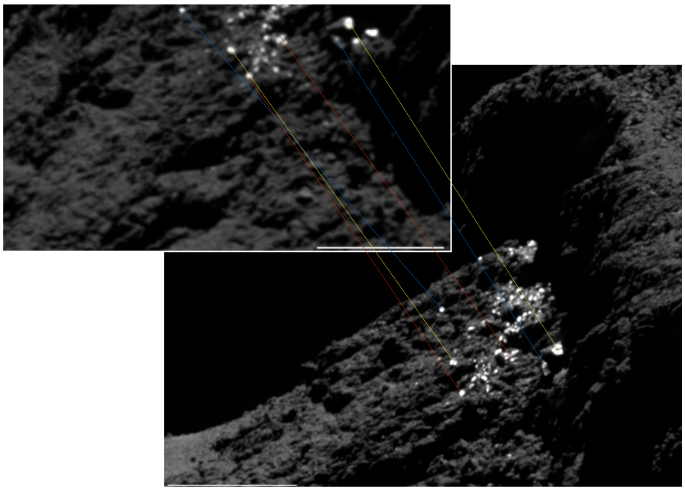

Fig. 6. Comparisons of OSIRIS NAC images of the cluster of bright spot 6, observed two months apart, which shows the stability of the bright features with time.

Table 6. Mass release rate of H_2O from the surface of 67P at the location of H_2O ice-rich spots.

Spot	T [K]	Q_{H_2O} [kg m^{-2} s^{-1}]	OSIRIS observations
1	203	3.357×10^{-4}	Size receded from 57 m to 36 m in 3 weeks
2	197	1.336×10^{-4}	Observed for 5 weeks
3	218	2.485×10^{-3}	Size receded from 18 m to 8 m in 3 weeks, disappear in the following 3 weeks
4	168	0.662×10^{-6}	Cluster stable for 11 weeks
5	188	3.003×10^{-5}	Stable for 13 weeks
6	179	0.625×10^{-5}	Cluster stable for 13 weeks
7	163	2.156×10^{-7}	Cluster stable for 3 weeks
8	158	0.701×10^{-7}	Stable for 15 weeks

Notes. In the last column an indication of the observed lifetime of the spots is summarised.

From the VIRTIS and OSIRIS data, we can measure several parameters: estimation of the amount of water ice on each spot, its local temperature, a timescale and an extent of erosion. These were measured at different times and should consequently be considered only as first order indications. They are theoretically linked together, so that we can use them to estimate whether ice behaves as expected for each spot. In Table 6 we report the mass release rate of H_2O (Prialnik et al. 2004), for each temperature, from the surface of 67P estimated in each of these locations as follows

$$Q_{H_2O} = \mathcal{P}_{H_2O}(T) \sqrt{\frac{m_{H_2O}}{2\pi k_B T}}, \quad (4)$$

with m_{H_2O} [kg] the mass of one molecule of H_2O, k_B the Boltzmann constant, T [K] the temperature of each spot, and $\mathcal{P}_{H_2O}$ the saturation vapor pressure, which can be written as

$$\mathcal{P}_{H_2O} = A e^{-B/T}, \quad (5)$$

with $A = 356 \times 10^{10}$ N m^{-2} and $B = 6141.667$ K for water (Fanale & Salvail 1984).

For each spot, the temperature changes because of local diurnal variations of the solar input, seasonal effects, shadowing, or self-heating. These effects are difficult to estimate since they depend on the local illumination geometry and thermophysical properties. A low thermal inertia, as derived by VIRTIS (Capaccioni et al. 2015) and MIRO (Schloerb et al. 2015), results in quite large day-night and seasonal variations of the temperature. These may influence the survival of ice-rich spots in a way that may be unpredictable. However, we find that the behavior of the eight spots found by the OSIRIS-VIRTIS study is in good agreement with the expected thermal behavior of H_2O ice.

Although the size and timescales measured for each spot may be considered with caution owing to the errors like those induced by shadows, they allow for another estimate of the mass release rate (Prialnik et al. 2004) through $Q_{H_2O} = \varrho\ \Delta l/\Delta t$, with ϱ the local density of water ice, Δl the typical extent of erosion of each spot, and Δt its erosion timescale. If we take the example of spot 1, the expected timescale to erode this feature at the observed extent and for a temperature of 203 K would be 50–100 h. We emphasize that given the numerous uncertainties this should be considered as a first order approximation. However, this timescale is such that the feature should be stable against day-night variations of the temperature, since it would take more than one cycle to erode it. In addition, the lower temperatures of the night would prevent such a rapid erosion. The total mass of water released by the erosion of spot 1 is $M = Q_{H_2O}\Delta t f \Delta S$ with ΔS the eroded surface and f the water ice fraction inferred from VIRTIS data modeling. The feature containing 1% of water ice seems to have decreased from 57 m to 36 m in about 22 days, i.e. ~1500 m^2 were eroded in $\sim 2 \times 10^6$ s. At 203 K, this translates into $\sim 10^4$ kg of water ice being sublimated, which is not possible to reach with surface ice alone. We thus have to assume that (1) icy grains may be scattered to the nucleus surface and recondence, creating a cycle maintaining water ice at the surface (Crifo 1987; Davidsson & Skorov 2004); (2) the average temperature is much lower than the temperature measured by VIRTIS; (3) ice-rich subsurface layers contribute to maintaining the surface ice. Case 1 is beyond the scope of the simple calculations we perform here. For case 2, we estimate that surface ice (contained in a 1 mm layer) would be able to reproduce the observed behavior if the average temperature is ~175 K: large day-night variations of the temperature would thus be necessary. For case 3, if we assume that subsurface layers have the same properties as the bulk of the comet, a layer of the order of ~10 cm would be required to explain the observed mass release. We note that in 67P, the diurnal and seasonal skin depths $\left(\left(\frac{P_{\rm spin}\kappa}{\pi\rho c}\right)^{1/2}\right.$ and $\left.\left(\frac{2\kappa a^{3/2}}{\sqrt{GM_\odot}\rho c}\right)^{1/2}\right.$, with a the semi major axis, c the specific heat, G the gravitational constant, κ the thermal conductivity, $M_\odot$ the solar mass, $P_{\rm spin}$ the spin period, and ρ the bulk density; Prialnik et al. 2004) vary from 1 mm to 9 cm and 80 cm to 7 m respectively, depending on local thermo-physical properties, as computed by Leyrat et al. (2015).

Spot 2 is larger than spot 1, but contains an order of magnitude less H_2O ice as inferred from spectral modeling. This feature's evolution is found to be in good agreement with the expected thermal behavior of water ice, as well as the inference from its low albedo that this spot is close to the end of the sublimation phase.

Spot 3 is the hottest feature measured in this study. If we assume that the ice-rich boulder has the same properties as the bulk of 67P, the 18 m feature being eroded in $\sim 3 \times 10^6$ s results in a mass release rate of 2.82×10^{-5} kg m^{-2} s^{-1}, i.e. two orders of magnitude less than the rate computed from the measured temperature. We should thus assume that the temperature is much lower most of the time at this spot, or the boulder properties vary from those of the bulk of the comet (a local density of 800 kg m^{-3} for example would be required). Alternatively, the very high temperature observed for spot 3 is likely the result of an areal mixture of icy and ice-free terrain within the VIRTIS pixel. Indeed, for a given observed albedo and temperature, the mixing of ice and dust at a grain level plays an important role: ice intimately mixed with dust will be hotter and shorter-lived than a patch of pure ice surrounded by dust. Given the low temperatures encountered for spots 4 to 8, it is expected that these features should be long-lived, as observed by OSIRIS and VIRTIS. At a lower temperature of 180 K (spot 6), the sublimation rate is only 0.625×10^{-5} kg m^{-2} s^{-1}, and decreases exponentially at lower temperatures (spots 4, 7, and 8).

The appearance of meter-sized spots, which are mostly only illuminated for a short fraction of the day, remains constant over time. These features would be more affected by seasonal variations than diurnal variations of the temperature, since water ice is mostly stable at the measured temperatures. Cometary activity, triggered below the surface by other volatile species, may locally influence the surface properties, such as the distribution of dust, and exposed fresh H_2O ice at the surface.

All the bright spots are on consolidated dust free materials, either on boulders or on freshly exposed outcropping regions that often display penetrative fractures. This suggests that H_2O ice can mainly be found on the consolidated substratum exposed along scarps or detached in the form of boulders. Some of the bright spots have been in place for weeks and months, while others seem related to diurnal variation.

7. Conclusions

Comet 67P/Churyumov-Gerasimenko shows a surface rich in heterogeneous geological structures and surface morphological variations that show color and albedo variations across the surface. The high-resolution images obtained by OSIRIS enable us to identify a large quantity of bright spots of different size and located in areas with different properties and high albedo.

In this paper, we present for the first time a complementary study of data acquired by the OSIRIS and VIRTIS instruments. A major objective of this paper is to firmly detect the presence of H_2O ice on the comet's surface. We confirm the presence of H_2O ice on eight new spots and we model the spectra with H_2O ice and dark material.

Comparing the coordinates of the detected eight H_2O ice spots with those of 67P dust jets, five spots (4, 5, 6, 7 and 8) have been found to lie in the approximate position of the jets identified by Vincent et al. (2016a) and one (spot 3) among the outbursts observed in the cometary summer (Vincent et al. 2016b). Observational evidence showed that the majority of dust jets also arose from rough terrains and fractured walls rather than smooth areas (Vincent et al. 2016a). Some of these detected H_2O ice spots have also been compared by Oklay et al. (2016b) to those of comets 9P and 103P.

The detection of H_2O ice signatures by VIRTIS on eight of the 13 locations given by OSIRIS data does not mean that the other spots do not contain ice on their surface and this can be explained by not simultaneous observations, unfavorable instrumental signal-to-noise conditions, spatial resolution on the surface, different illumination/viewing geometry, and by the fact that VIRTIS-M channel was unavailable after 4 May, 2015 owing to the failure of the active cooler.

The main results of this work can be summarized as follows:

- We presented for the first time a complementary analysis of H_2O ice-rich areas using data acquired by the OSIRIS and VIRTIS instruments. Comparing high spatial resolution VIS images with extended IR range spectra enables us to study the morphological, thermal and compositional properties of these areas at the same time.
- The analysis of the spectral properties observed by VIRTIS-M indicates that, on these areas, the H_2O ice abundance is between 0.1 and 7.2%, mixed in areal or/and in intimate modalities with the dark terrain.
- The ice is distributed on the two lobes of 67P in locations which remain in shadow for longer.
- The detected bright spots are mostly on consolidated dust free material surfaces, mostly concentrated in equatorial latitudes.
- The mass release of H_2O at the location of the eight ice-rich spots has been estimated.
- Some spots are stable for several months and others show temporal changes connected to diurnal and seasonal variations. Stability of the spots is corroborated by the temperature retrieved at the surface. The behavior of ice on these locations is in very good agreement with theoretical expectations.
- Six of the detected H_2O ice spots are located in approximately the same position of the previously detected cometary jets.

H_2O ice is present on the surface substrata where solar illumination plays an important role with seasonal and diurnal variations. During the perihelion orbit passage of the comet, the Rosetta spacecraft was at a greater distance and the available surface OSIRIS images were at lower resolution. Starting in March 2016, the comet is observed again from close distances. With analysis of other available data (in particular from OSIRIS), we will study the surface changes after the perihelion passage to better understand the surface evolution of the comet.

Acknowledgements. OSIRIS was built by a consortium of the Max-Planck-Institut für Sonnensystemforschung, Göttingen, Germany, CISAS-University of Padova, Italy, the Laboratoire d'Astrophysique de Marseille, France, the Instituto de Astrofísica de Andalucia, CSIC, Granada, Spain, the Research and Scientific Support Department of the European Space Agency, Noordwijk, The Netherlands, the Instituto Nacional de Técnica Aeroespacial, Madrid, Spain, the Universidad Politéchnica de Madrid, Spain, the Department of Physics and Astronomy of Uppsala University, Sweden, and the Institut für Datentechnik und Kommunikationsnetze der Technischen Universität Braunschweig, Germany. VIRTIS was built by a consortium from Italy, France, and Germany, under the scientific responsibility of IAPS, Istituto di Astrofisica e Planetologia Spaziali of INAF, Rome, which lead also the scientific operations. The VIRTIS instrument development for ESA has been funded and managed by ASI (Italy), with contributions from Observatoire de Meudon (France) financed by CNES and from DLR (Germany). The VIRTIS instrument industrial prime contractor was former Officine Galileo, now Finmeccanica in Campi Bisenzio, Florence, Italy. The support of the national funding agencies of Germany (DLR), France (CNES), Italy (ASI), Spain (MEC), Sweden (SNSB), and the ESA Technical Directorate is gratefully acknowledged.

References

Acton, C. H. 1996, Planet. Space Sci., 44, 65
Auger, A.-T., El-Maarry, M. R., Groussin, O., et al. 2015, A&A, 583, A35
Barucci M. A., Dotto, E., & Levasseur-Regourd, A. C. 2011, A&ARv, 19, 48
Bockelée-Morvan, D., Debout, V., Erard, S., et al. 2015, A&A, 583, A6
Capaccioni, F., Coradini, A., Filacchione, G., et al. 2015, Science, 347, 0628
Ciarniello, M., Capaccioni, F., Filacchione, G., et al. 2011, Icarus, 214, 541
Ciarniello, M., Capaccioni, F., Filacchione, G., et al. 2015, A&A, 583, A31
Clark, R. N., Cruikshank, D. P., Jaumann, R., et al. 2012, Icarus, 218, 831
Coradini, A., Capaccioni, F., Drossart, P., et al. 2007, Space Sci. Rev., 128, 529
Crifo, J. F. 1987, A&A, 187, 438
Davidsson, B. R. J., & Skorov, Y. V. 2004, Icarus, 168, 163
De Sanctis, M. C., Capaccioni, F., Ciarniello, M., et al. 2015, Nature, 525, 500
El-Maarry, M. R., Thomas, N., Giacomini, L., et al. 2015, A&A, 583, A26
El-Maarry, M. R., Thomas, N., Gracia-Berna, A., et al. 2016, A&A, 593, A110
Fanale, F. P., & Salvail, J. R. 1984, Icarus, 60, 476
Filacchione, G., De Sanctis, M. C., Capaccioni, F., et al. 2016a, Nature, 529, 368
Filacchione, G., Capaccioni, F. Ciarniello, M., et al. 2016b, Icarus, 274, 334
Fornasier, S., Hasselmann, P. H., & Barucci, M. A., et al. 2015, A&A, 583, A30
Fornasier, S., Mottola, S., Keller, H. U, et al. 2016, Science, submitted
Groussin, O., Sierks, H., & Barbieri, C. 2015, A&A, 583, A36
Hapke, B. 2012, Theory of reflectance and emittance spectroscopy (Cambridge University, Press)
Jorda, L., Spjuth, S., Keller, H. U, et al. 2010, Proc. SPIE, 7533, 753311
Jorda, L., Gaskell, R. W., Capanna, C., et al. 2016, Icarus, 277, 257
Keller, H. U., Barbieri, C., Lamy. P. L., et al. 2007, Space Sci. Rev., 128, 26
Leyrat, C., Tosi, F., Capaccioni, F., et al. 2015, Europ. Planetary Science Congress 2015, 435
Li, J.-Y., Besse, S., A' Hearn, M. F., et al. 2013, Icarus, 222, 559
Mastrapa, R. M., Bernstein, M. P., Sandford, S. A., et al. 2008, Icarus, 197, 307
Mastrapa R. M., Bernstein, M. P., Sandford, S. A., et al. 2009, ApJ, 701, 1347
Migliorini, A., Piccioni, G., Capaccioni, F., et al. 2016, A&A, 589, A45
Oklay, N., Vincent, J.-B., Fornasier, S., et al. 2016a, A&A, 586, A80
Oklay, N., Sunshine, J. M., Pajola, M., et al. 2016b, MNRAS, submitted
Pajola, M., Vincent, J.-B., Guttler, C., et al. 2015, A&A, 583, A37
Pommerol, A., Thomas, N., El-Maarry, M. R., et al. 2015, A&A, 583, A25
Preusker, F., Scholten, F., Matz, K.-D., et al. 2015, A&A, 583, A33
Prialnik, D., Benkhoff, J., & Poddak, M. 2004, in Comets II, eds. M. C. Festou, H. U. Keller, & H. A. Weaver (Univ. of Arizona Press), 359
Protopapa, S., Sunshine, J. M., Feaga, L. M., et al. 2014, Icarus, 238, 191
Quirico, E., Moroz, L. V., Schmitt, B., et al. 2016, Icarus, 272, 32
Raponi, A., 2014, Ph.D. Thesis, Università degli studi di Roma Tor Vergata [arXiv:1503.08172]
Raponi, A., Ciarniello, M., Capaccioni, F., et al. 2016, MNRAS, submitted
Reinhard, R., & Battrick, B. 1986, ESA SP, 1077
Schloerb, F. P., Keihm, S., von Allmen, P., et al. 2015, A&A, 583, A29
Sierks, H., Barbieri, C., Lamy, P., et al. 2015, Science, 347, 1044
Sunshine, J. M., A'Hearn, M. F., Groussin, O., et al. 2006, Science, 311, 1453
Sunshine, J. M., Feaga, L. M., Groussin, O., et al. 2012, LPI Contribution, 1667, 6438
Thomas, N., Sierks, H., Barbieri, C., et al. 2015a, Science, 347, 440
Thomas, N., Davidsson, B., El-Maarry, M. R., et al. 2015b, A&A, 583, A17
Tosi, F., Capria, M. T., De Sanctis, M. C., et al. 2014, Icarus, 240, 36
Tubiana, C., Kovacs, G., Guttler, C., et al. 2015, A&A, 583, A46
van der Walt, S., Schonberger, J. L., Nunez-Iglesias, J., et al. 2014, Scikit-image: Image processing in Python. PeerJ 2:e453, http://dx.doi.org/10.7717/peerj.453
Vincent, J.-B., Bodewitz, D., & Besse, S. 2015, Nature, 523, 63
Vincent, J.-B., Oklay, N., Pajola, M., et al. 2016a, A&A, 587, A14
Vincent, J.-B., A'Hearn, M. F., Lin, Z.-Y., et al. 2016b, MNRAS, submitted
Warren, S. G. 1984, Appl. Opt., 23, 1206

[1] LESIA, Observatoire de Paris, CNRS, UPMC Univ. Paris 06, Univ. Paris-Diderot, 5 Place J. Janssen, 92195 Meudon Principal Cedex, France
e-mail: antonella.barucci@obspm.fr
[2] INAF-IAPS, 00133 Rome, Italy
[3] Univ. Paris Diderot, Sorbonne Paris Cité, 4 rue Elsa Morante, 75205 Paris Cedex 13, France
[4] Max-Planck-Institut für Sonnensystemforschung, Justus-von-Liebig-Weg 3, 37077 Göttingen, Germany
[5] Physikalisches Institut, Sidlerstrasse 5, University of Bern, 3012 Bern, Switzerland
[6] Dipartimento di Geoscienze, University of Padova, 35122 Padova, Italy
[7] Observatoire des Sciences de l'Univers, 25000 Besançon, France
[8] Department of Physics and Astronomy "G. Galilei", University of Padova, Vic. Osservatorio 3, 35122 Padova, Italy
[9] Laboratoire d'Astrophysique de Marseille, UMR 7326, CNRS & Aix Marseille Université, 13388 Marseille Cedex 13, France
[10] Centro de Astrobiología, CSIC-INTA, 28850 Torrejón de Ardoz, Madrid, Spain

[11] International Space Science Institute, Hallerstrasse 6, 3012 Bern, Switzerland
[12] Research and Scientific Support Department, European Space Agency, 2201 Noordwijk, The Netherlands
[13] Department of Physics and Astronomy, Uppsala University, 75120 Uppsala, Sweden
[14] PAS Space Research Center, Bartycka 18A, 00716 Warszawa, Poland
[15] Institute for Geophysics and Extraterrestrial Physics, TU Braunschweig, 38106 Braunschweig, Germany
[16] Department for Astronomy, University of Maryland, College Park, MD 20742-2421, USA
[17] Institute of Planetary Research, DLR, Rutherfordstrasse 2, 12489 Berlin, Germany
[18] LATMOS, CNRS/UVSQ/IPSL, 11 Boulevard d'Alembert, 78280 Guyancourt, France
[19] INAF–Osservatorio Astronomico di Padova, Vicolo dell'Osservatorio 5, 35122 Padova, Italy
[20] Department of Information Engineering - University of Padova, via Gradenigo 6, 35131 Padova, Italy
[21] JPL, 4800 Oak Grove Drive, Pasadena, CA91109, USA
[22] Dipartimento di Fisica, Universita del Salento, Italy
[23] INAF–Osservatorio Astronomico di Trieste, via Tiepolo 11, 34143 Trieste, Italy
[24] Institute for Space Science, National Central University, 32054 Chung-Li, Taiwan
[25] ESA/ESAC, PO Box 78, 28691 Villanueva de la Cañada, Spain
[26] Instituto de Astrofísica de Andalucía – CSIC, 18080 Granada, Spain
[27] NASA Ames Research Center, CA 94035, USA
[28] UJF-Grenoble 1/CNRS-INSU, 38400 Saint Martin d'Hères, France